


## Research Article

# Ultrasonic Time-Frequency Response Characteristics for Damage Evolution of Back-Filling Concrete under Staged Loading Conditions

Xicai Gao <sup>1,2</sup>, Xichen Zhang,<sup>1,2</sup> Cheng Zhao,<sup>1,2</sup> Huan Xia,<sup>1,2</sup> Shuai Liu,<sup>1,2</sup> Tengfei Ma,<sup>1,2</sup> Jianhui Yin,<sup>3</sup> and Kai Fan<sup>4</sup>

<sup>1</sup>*Xi'an University of Science and Technology, State Key Laboratory of Coal Resources in Western, Xi'an, China*

<sup>2</sup>*Xi'an University of Science and Technology, Key Laboratory of Western Mine Exploitation and Hazard Prevention, Ministry of Education, Xi'an, Shaanxi 710054, China*

<sup>3</sup>*Shaanxi Coal and Chemical Technology Institute Co Ltd, Xi'an, Shaanxi 710065, China*

<sup>4</sup>*Sichuan Coal Industry Group Huarong Co Ltd, Lushuidong Coal Mine, Guangan, Sichuan 638500, China*

Correspondence should be addressed to Xicai Gao; [gxcai07@163.com](mailto:gxcai07@163.com)

Received 3 March 2022; Revised 20 May 2022; Accepted 21 June 2022; Published 14 July 2022

Academic Editor: Chang Chuan Lee

Copyright © 2022 Xicai Gao et al. This is an open access article distributed under the Creative Commons Attribution License, which permits unrestricted use, distribution, and reproduction in any medium, provided the original work is properly cited.

Under the influence of repeated mining disturbance, the back-filling body for the gob-side entry retaining may experience a reduction in the bearing capacity or even failure, complicating the control of surrounding rock stability in coal mines. This study employs an electro-hydraulic three-axis servo testing machine and an ultrasonic detection system to study damage evolution and the precursor instability response behavior of the back-filling concrete of the gob-side entry retaining. Specifically, we conduct staged loading experiments on the specimens of back-filling concrete. By analyzing the characteristic stress of the concrete specimens and the ultrasonic time-frequency response characteristics, we explore the damage evolution and bearing capacity deterioration process. Results show that under staged loading conditions, the concrete specimens underwent a differential change process from nonuniform to uniform deformation, to localized deformation, and finally to failure. The velocity of the ultrasonic wave of the loaded concrete specimens first increased, then decreased with increasing stress, and the macroscopic deformation characteristics were consistent with damage development and evolution, showing clear stage-specific characteristics. The ultrasonic time-frequency response characteristics of the loading process characterized damage accumulation in the concrete specimens, loading state variation, and the deterioration of load-bearing capacity in great detail. During the staged loading process, the attenuation coefficient was positively correlated to bearing capacity, and the coefficient of variation (CV) of the dominant frequency was inversely proportional to the degree of crack development. Compared with the ultrasonic wave velocity, the time-frequency response characteristics were more sensitive to damage evolution. In summary, our findings provide an experimental basis for long-term stability monitoring and evaluation of the back-filling body for gob-side entry retaining in coal mines.

## 1. Introduction

The technique of gob-side entry retaining refers to the construction of artificial walls (i.e., back-filling bodies) at the edges of a mined-out area after the advancement of the working face in the upper section. It serves to retain the mining roadway of the working face in the lower section and to use it as the mining roadway in that section. It is a pillar-

free mining technology. As the gob-side entry retaining technique has the advantages of avoiding gas accumulation, alleviating the tension of mining replacement, and yielding better coal recovery rates, it has been widely used in the mining of thin, medium, and thick coal seams in recent years. This technique is a key development direction for mining roadway protection in China [1–5]. The back-filling body is constantly affected by repeated disturbances from

the roof subsidence of the mined-out area in the current section and the advancement of the working face in the lower section. It is common for the back-filling body to have reduced load-bearing capacity and even to fail, which brings great challenges to the control of the rock surrounding gob-side entry retaining. [6] Therefore, the stability of the back-filling body is key to the success of roadway protection in the gob-side entry retaining technique.

Promising outcomes have been obtained in research on the stress and deformation characteristics of the back-filling body for gob-side entry retaining under the influence of mining. For example, Huang et al. [7] studied mine pressure on the section of gob-side entry retaining and analyzed the deformation and stress characteristics of the back-filling body. Jia-guang et al. [8] established a stacked continuous slab model under different roof conditions and proposed a formula for the support resistance of the back-filling body. Guorui et al. [9] reported that the stress and deformation of the back-filling body for gob-side entry retaining in thick coal seams was directly related to the roof failure of the working face, and as the working face advanced, stress, firstly, increased and then became stable. Chen et al. [10] showed that the back-filling body was loaded not only by the dominant roof and the immediate roof but also by roof displacement following the fracture of the dominant roof. It results in the generation, development, and penetration of cracks on both sides of the body, greatly affecting the integrity and bearing capacity of the back-filling body. Han et al. [11] found that the roof movement after the fracture in the mined-out area is a key influencing factor for gob-side entry retaining. These authors presented the characteristics of a staged collapse of the overlying rock in the mined-out area and its disturbance on gob-side entry retaining. Then, they proposed a calculation method for the load of the back-filling wall and reinforcement measures. In addition, Shengpeng [12] studied the influence of the buried depth of the roadway, roof thickness, and the location of the main roof fracture on the stability of the back-filling body. These authors further proposed a stability reinforcement technology for the back-filling body [13, 14]. In summary, existing studies focus mainly on stress distribution, deformation, and the reinforcement of the back-filling body. Cumulative damage, progressive failure process, and the instability prediction of the back-filling concrete body in gob-side entry retaining under the influence of mining should be further studied.

The failure of the back-filling body for gob-side entry retaining refers to a process involving internal crack closure, initiation, and development until the macroscopic failure of the back-filling concrete. This process is closely related to the roof fracture, mining state, and the damage evolution of the back-filling concrete. This study examines the characteristics of the damage evolution of the back-filling concrete under the influence of mining. The stress-strain state of the back-filling concrete was analyzed based on ultrasonic characteristic parameters. This study is of great significance and engineering practice value to realize the intelligent monitoring and evaluation of the stable state of the back-filling body for gob-side entry retaining.

TABLE 1: Composition of the concrete mix.

| Component type                   | Dosage |
|----------------------------------|--------|
| P. O42.5                         | 850 kg |
| Sand (0 ~ 5 mm)                  | 700 kg |
| Gravel (5 ~ 15 mm)               | 850 kg |
| Water                            | 325 kg |
| Admixtures (waterproofing agent) | 1.3 kg |
| W/C ratio                        | 0.38   |

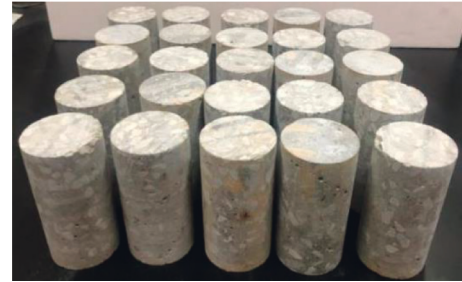


FIGURE 1: Concrete sample.

## 2. Damage Evolution of Back-Filling Concrete for Gob-Side Entry Retaining under Staged Loading Conditions

**2.1. Specimens.** The back-filling concrete material is composed of Portland cement, river sand (0 ~ 5 mm), gravel (5 ~ 15 mm), and admixtures (waterproofing agent). According to the back-filling concrete formula of gob-side entry retaining in field engineering example, cement, sand (0 ~ 5 mm), gravel (5 ~ 15 mm), admixtures, and water were mixed with a mass ratio of 1 : 0.82 : 1 : 0.38 and then poured into a mold (Table 1) after mixing, vibration, consolidation, curing, and other processes, and the back-filling concrete cylindrical samples were prepared through dry drilling, cutting, and grinding according to the method recommended by the national standard. The diameter of the cylindrical samples is 50 mm, the height is 100 mm (Figure 1), the diameter error is within 0.3 mm, and the surface smoothness controlled is within 0.02 mm. The sample size and precision meet the international rock mechanics test standards. The specimens were cured in a cool, dry, ventilated place for 28 days. The average initial wave velocity of the specimens was 3209 m/s, and the density was 2290 kg/m<sup>3</sup>.

**2.2. Test Equipment.** The uniaxial compression test was carried out using the MTS815 Flex Test GT system (Figures 2 and 3) with an axial load capacity of 2300 kN, sensitivity of the servo valve of 290 Hz, a data acquisition frequency of 5 kHz, and a strain rate range of  $10^{-6} \sim 10^{-1}$ . The specimens were loaded in the axial displacement or load control mode, and load and displacement data during the loading process were collected. Axial deformation was measured using an LVDT displacement sensor, and lateral deformation was measured via the elongation of the ring-shaped chain



FIGURE 2: Uniaxial loading of concrete sample.

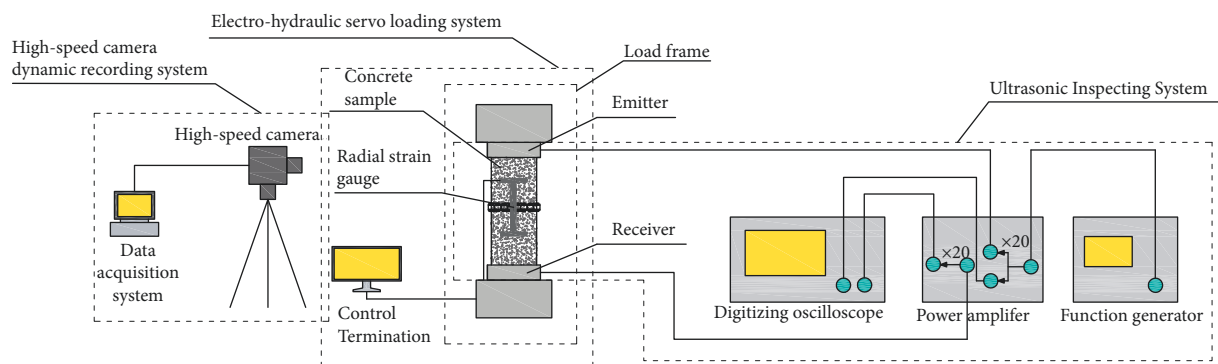


FIGURE 3: Integrated test system construction.

clamped in the middle of the specimen. Test accuracy was 0.001 mm.

The ultrasonic testing system (Figure 4) comprises a waveform signal generator (Key sight), high-frequency, high-voltage amplifier (Olympus), oscilloscope (Key sight), and two transducers. The diameter of the transducer is 60 mm, the maximum pressure is 50 MPa, and the resonance frequency is 55 kHz. The damping of the ultrasonic transmitting and receiving transducers met the requirements for concrete mechanical testing.

The signal generator was used to generate the ultrasonic signals of different frequencies and amplitudes, and the oscilloscope realized the functions of ultrasonic wave arrival correction, spectrum analysis, and display.

### 2.3. Experimental Scheme

**2.3.1. Determine the Loading Path.** Taking the geological conditions of gob-side entry retaining in  $X$  working face of a coal mine as background, a three-dimensional numerical calculation model of gob-side entry retaining under the

influence of mining was established. The  $FLAC^{3D}$  model was generated using the generate command. The size was  $X$  (length)  $\times Y$  (width)  $\times Z$  (height) = 315 m  $\times$  300 m  $\times$  48.3 m. The Mohr-Coulomb yield criterion was used in the calculation model. Gravity stress of roof 7.76 MPa was applied to the upper boundary of the model. In the model, the bottom of the model constrains the vertical displacement, and the front, the back, and the side of the model constrain the horizontal displacement. The coal seam is simplified as a horizontal arrangement. The thickness of the coal seam is 3.35 ~ 6.76 m, with an average of 6.09 m. The roof and floor are mainly made of mudstone and siltstone. The gob-side entry retaining along the gob is arranged in the middle of the model along the floor. The height and width of the roadway are 3200 mm and 5800 mm, and the width of the back-filling body beside the roadway is 1400 mm in Figure 5.

The stress distribution of the back-filling body at different positions under the influence of mining is shown in Figure 6.

With the advance of the working face, the vertical stress of the back-filling body at different positions is obviously different. The maximum stress is in the middle of the back-

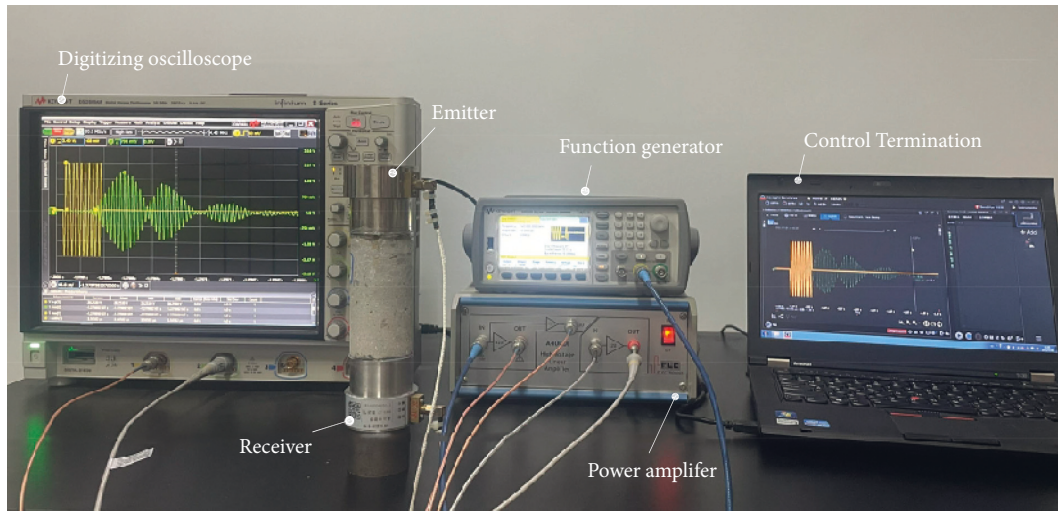


FIGURE 4: Diagram of ultrasonic testing system.

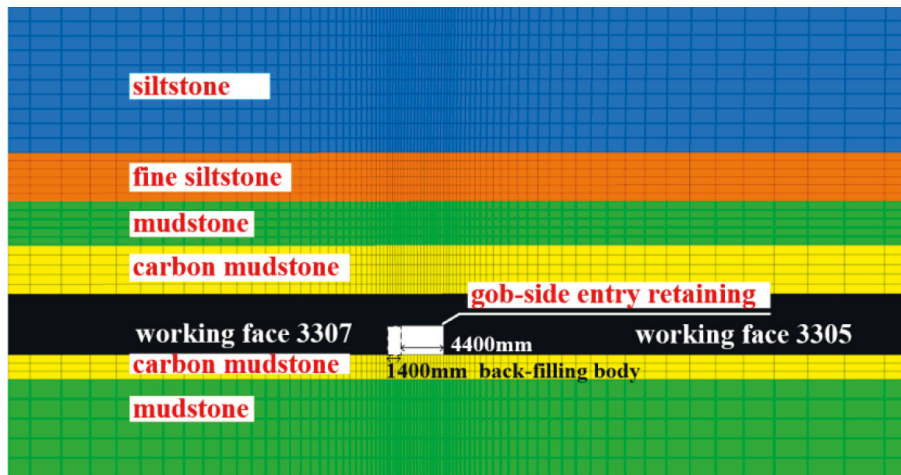


FIGURE 5: Numerical calculation model.

filling body, followed by the side of the gob, and the minimum stress is in the side of the roadway. Under the influence of mining, the vertical stress of the back-filling body increases monotonously in the early stage and gradually becomes stable in the later stage on the whole. The numerical simulation results are basically consistent with the field measurement results in literature [7, 9]. Hence, the evolution process of the real stress environment of the back-filling body is simplified as staged loading.

**2.3.2. Loading Scheme.** The specimens were loaded under staged loading conditions at a rate of 5 kN/s using the MTS815 rock mechanics system. After loading in each stage, the maximum load was kept constant for 20 s, during which the ultrasonic test was carried out. The loading cycle was repeated until the failure of the specimen. In the ultrasonic test, the transducers were placed on the upper and lower ends of the specimens; one served as the exciter and the other was the receiver. Ultrasonic complaints were applied to the

surface to ensure good contact between the specimen and the transducers. The waveform generator emitted a high-voltage pulse signal, and the excitation frequency of the ultrasonic wave was 140 kHz. The amplitude of the pulse signal was 10 V<sub>pp</sub>, and the output voltage was 200 V<sub>pp</sub> after passing through the amplifier. The vibration propagated in the specimen and was received by the transducer on the other end. The data acquisition frequency of the wave recorded by the oscilloscope is 5 MHz.

### 3. Results

**3.1. Compression Deformation and Characteristic Stress.** The back-filling concrete is a sand-gravel mixture with inevitable micropores, cracks, joints, and other microdefects from the process of slurry compaction, specimen preparation, and curing. As the stress increased during the staged loading process, there was the closure, expansion, connection, and penetration of internal microcracks, ultimately forming macroscopic cracks and a specimen fracture. The

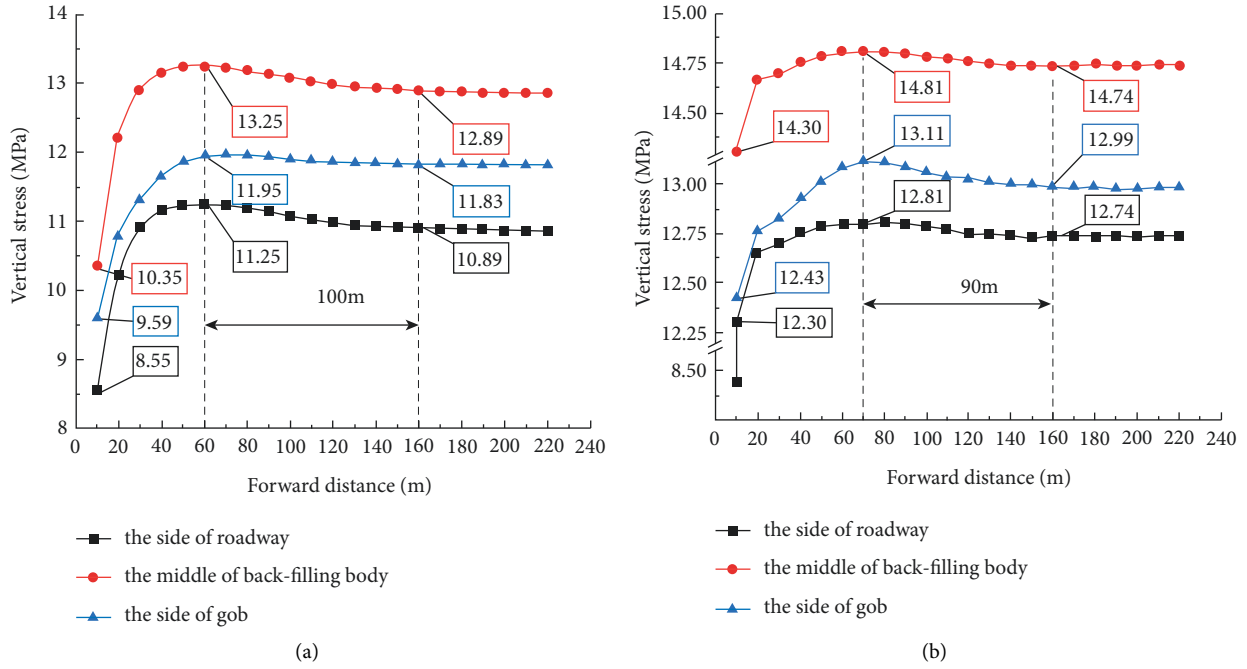


FIGURE 6: The stress distribution of the back-filling body under the influence of mining. (a) First mining. (b) Secondary mining.

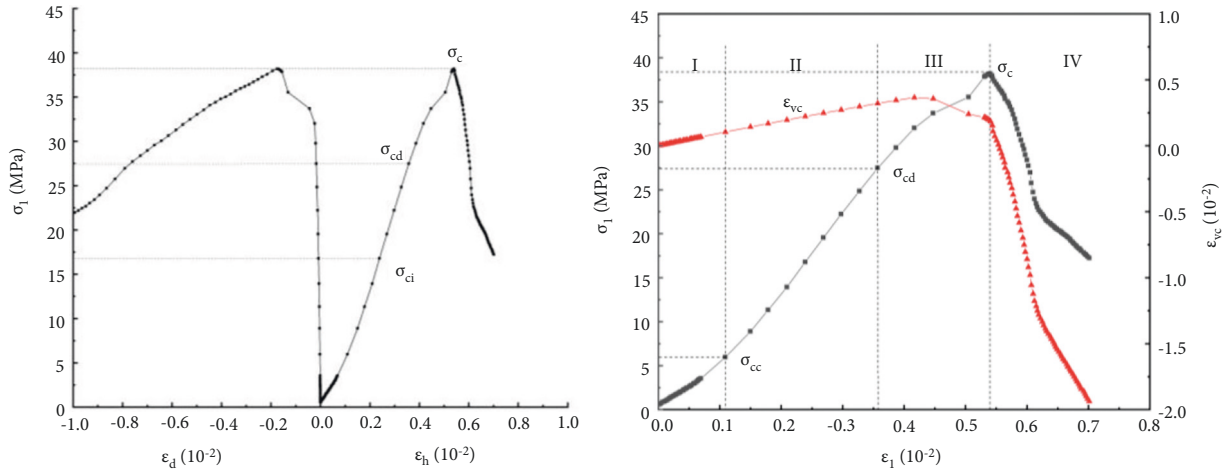


FIGURE 7: Stress-strain curve in uniaxial compression test and characteristic stress.

compression deformation of the specimens can be divided into four stages: crack compaction stage (I), elastic stage (II), plastic stage (III), and postfailure stage (IV). The stress-strain curve of the back-filling concrete specimens is shown in Figure 7.

According to the determination method of the characteristic stress proposed in reference [15–17], the crack initiation stress  $\sigma_{ci}$ , damage stress  $\sigma_{cd}$ , and peak stress  $\sigma_c$  of back-filling concrete under uniaxial compression are obtained. The results are shown in Table 2. The crack initiation stress  $\sigma_{ci}$  is the axial stress corresponding to the initial offset point at the end of the horizontal segment of the volumetric strain curve, and the damage stress  $\sigma_{cd}$  is the axial stress corresponding to the inflection point of the volumetric strain curve.

TABLE 2: Characteristic stress value in the process of graded loading of concrete sample.

| Specimen | $\sigma_c$ (MPa) | $\sigma_{cc}$ (MPa) | $\sigma_{cd}$ stress ratio (%) | $\sigma_{cd}$ (MPa) | $\sigma_{cc}$ stress ratio (%) |
|----------|------------------|---------------------|--------------------------------|---------------------|--------------------------------|
| D-1      | 47.88            | 6.30                | 13.16                          | 39.35               | 82.18                          |
| D-2      | 41.30            | 6.57                | 15.90                          | 33.38               | 80.82                          |
| D-3      | 38.16            | 5.96                | 26.20                          | 27.48               | 71.99                          |
| D-4      | 39.04            | 6.92                | 17.73                          | 30.36               | 77.76                          |

Because of space limitations, only specimen #3 is described here as an example. In the initial stage, the original pores and cracks in the concrete specimen slowly closed, and the stress-strain curve was concave. The elastic modulus increased with an increased load, and lateral strain  $\epsilon_d$

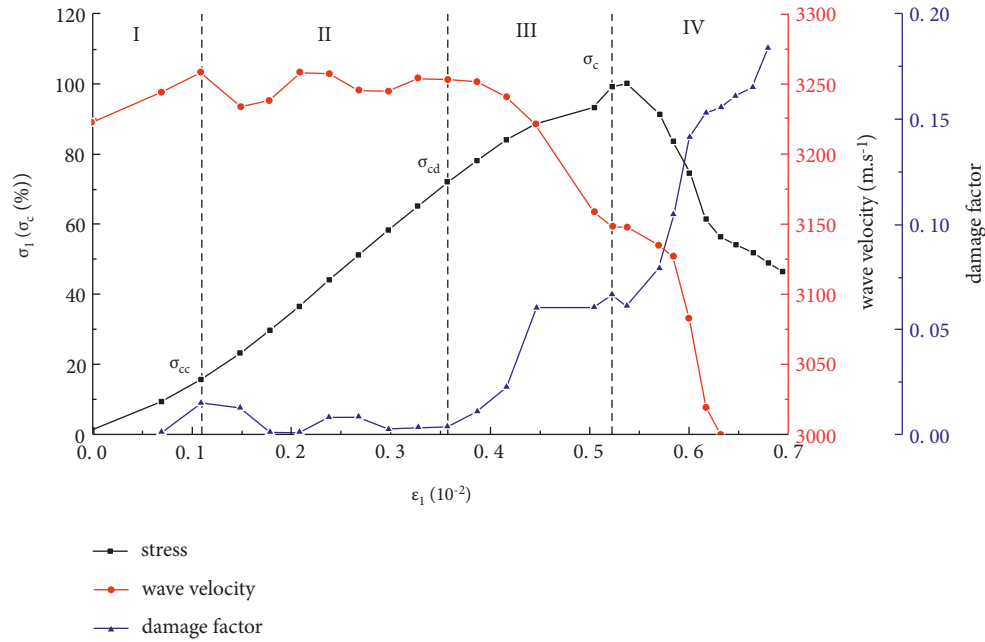


FIGURE 8: Relationships between ultrasonic wave velocity, damage, and stress.

increased insignificantly. When the load reached 5.96 MPa, the axial strain  $\varepsilon_h$  was 0.10%, the growth rate of the elastic modulus decreased, and the minimum volumetric strain was obtained. At this point, the crack compaction stage was completed. Closure stress  $\sigma_{cc}$  was 15.6% of peak stress  $\sigma_c$ . As the load continually increased, deformation entered the elastic deformation stage, the elastic modulus remained basically unchanged, and the stress-strain curve became linear. Crack volume strain began to increase. When the load reached 16.78 MPa, the axial strain  $\varepsilon_h$  was 0.24%, and internal cracks began to grow. At this point, crack-initiation stress  $\sigma_{ci}$  was 43.9% of peak stress  $\sigma_c$ . As the load further increased, lateral strain  $\varepsilon_d$  continued to increase, and the specimen deformation entered the crack-expansion stage. When the load reached 27.48 MPa, the axial strain  $\varepsilon_h$  was 0.36%, and the stress-strain curve began to deviate from the straight line. The growth rate of the crack volume strain  $\varepsilon_{vc}$  slowed, and the internal cracks expanded unsteadily. The volume strain increment gradually decreased to 0, and the specimen reached damage stress  $\sigma_{cd}$  or 72.0% of peak stress  $\sigma_c$ . In the plastic deformation stage, the internal cracks further developed. When the load increased to 38.16 MPa, the axial strain  $\varepsilon_h$  was 0.54%, which was manifested by a large increase in the lateral strain  $\varepsilon_{vc}$  and volume expansion. The specimens showed localized deformation and a macroscopic penetration of cracks, shear slippage, and tensile-shear composite failure. The load-bearing capacity of the specimen deteriorated while the section remained intact.

### 3.2. Ultrasonic Response Characteristics of the Damage Evolution Process of Back-Filling Concrete

**3.2.1. Variation of Ultrasonic Wave Velocity.** Ultrasound is a type of sound wave. It is generated by vibrations and

propagates in back-filling concrete. When encountering discontinuous or heterogeneous interfaces, such as fissures or cracks, the ultrasonic wave is reflected and refracted, resulting in changes in the waveform and wave velocity [18]. The damage variable introduced in this study is based on the phenomenological method of damage mechanics, and the relationship between ultrasonic wave velocity and the damage variable of the specimens was established such that the degree of damage of the concrete specimens was indirectly measured by the ultrasonic wave velocity. The concrete damage factor based on ultrasonic wave velocity is as follows [19]:

$$D = 1 - \frac{V^2}{V_0^2} \quad (1)$$

where  $D$  is the damage factor,  $V_0$  is initial wave velocity, and  $V$  is the velocity in the damaged specimens.

The relationship between the ultrasonic wave velocity and stress at different loading levels is shown in Figure 8. Note that the longitudinal wave velocity is closely related to the degree of the development of pores and cracks in the specimens. At the initial stage of loading, the internal pores and cracks of the specimen were closed because of compaction, and the ultrasonic wave velocity increased linearly to its maximum. At this point, closure stress was 5.96 MPa, which is consistent with closure stress  $\sigma_{cc}$  above. Taking specimen 3 as an example, as the stress increased, the specimen entered the elastic deformation stage. Because of the small number of internal cracks in the specimen, the wave velocity fluctuated only in a small range, indicating a low degree of damage. In the first part of the elastic deformation stage, subsidence was clearly noted and possibly caused by the irregular dislocation and uniform deformation of the internal particles of the specimen. In the later part of

this stage, wave velocity was relatively stable and showed a downward trend. Internal fissures began to develop and expand, and the damage value increased. At this point, the stress value reached 27.48 MPa, the specimen reached damage stress  $\sigma_{cd}$ , and the stress value was 72.0% of peak stress  $\sigma_c$ . In the plastic deformation stage, the ultrasonic wave velocity continued to decrease after experiencing a brief period of fluctuation, the damage value increased greatly, and the magnitude of subsidence significantly increased. Moreover, the cracks further expanded to form a through crack, and the damage value increased sharply. At this point, the stress value reached 37.84 MPa or 99.2% of peak stress  $\sigma_c$ . The specimen showed shear failure, and the load-bearing capacity of the specimen deteriorated.

During the staged loading process, ultrasonic wave velocity first increased and then decreased with increasing stress. The difference in ultrasonic wave velocity at different stress levels is reflected mainly in the change trend and amplitude. The ultrasonic wave velocity increased linearly to its maximum value at the initial stage of loading. When the fissures closed and the specimen entered the elastic deformation stage, the wave velocity began to decrease significantly. When peak stress was reached, the wave velocity fluctuated for a short time and then continued to decrease at a more rapid rate, and the damage value increased sharply. The macroscopic manifestation was that the cracks expanded to form a through crack. The damage factor determined by the wave velocity was consistent with the characteristics of the stress-strain curve. Therefore, the ultrasonic parameters reflect the crack propagation and damage evolution process of a back-filling body under loading. Moreover, the ultrasonic wave velocity was more sensitive to the stress state and strain characteristics of the specimen. The wave velocity decline trend and amplitude can be used as the criteria for stage division and failure prediction.

### 3.2.2. Ultrasonic Time-Frequency Response Parameters and Variation

(1) *Attenuation Coefficient.* When an ultrasonic wave propagates in the concrete medium, the ultrasonic signal carries a lot of information reflecting the characteristics of the concrete medium. When the composition of the back-filling concrete changes, acoustic impedance also changes, along with the development of the internal cracks under different stress levels. When propagating in the concrete specimens, the ultrasonic wave is diffracted or reflected, causing energy attenuation and spectrum distortion of the signal. At each loading level, the stress remains unchanged for a short period for the transducers to transmit and receive pulse signals. Based on a frequency-based exponential model, energy attenuation when the ultrasonic wave propagates from  $d_0$  to  $d$  is expressed as follows:

$$|p| = |p_0| e^{\alpha(f,d,d_0)}, \quad (2)$$

where  $p_0$  is the sound pressure at  $d_0$ , and  $p$  is the sound pressure at  $d$ .  $\alpha(f,d,d_0)$  is the attenuation coefficient at  $d$  when the frequency is  $f$ , with  $d_0$  as the reference position.

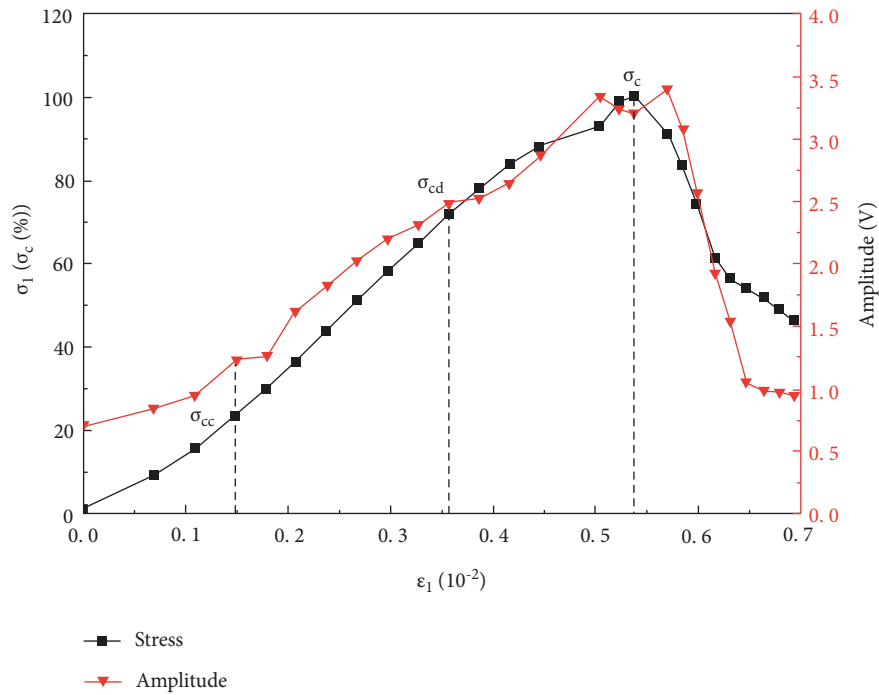
In the tests, the pressure and degree of coupling were kept unchanged, and the ultrasonic sound pressure was proportional to amplitude. The ratio of the amplitude of the received pulse signal before and after the staged loading was taken as a replacement for the sound pressure ratio, and the logarithm of the ratio was taken as the attenuation coefficient. Thus, the calculation equation of attenuation coefficient  $\alpha$  is as follows:

$$\alpha = \frac{(\ln A - \ln A_0)}{d}, \quad (3)$$

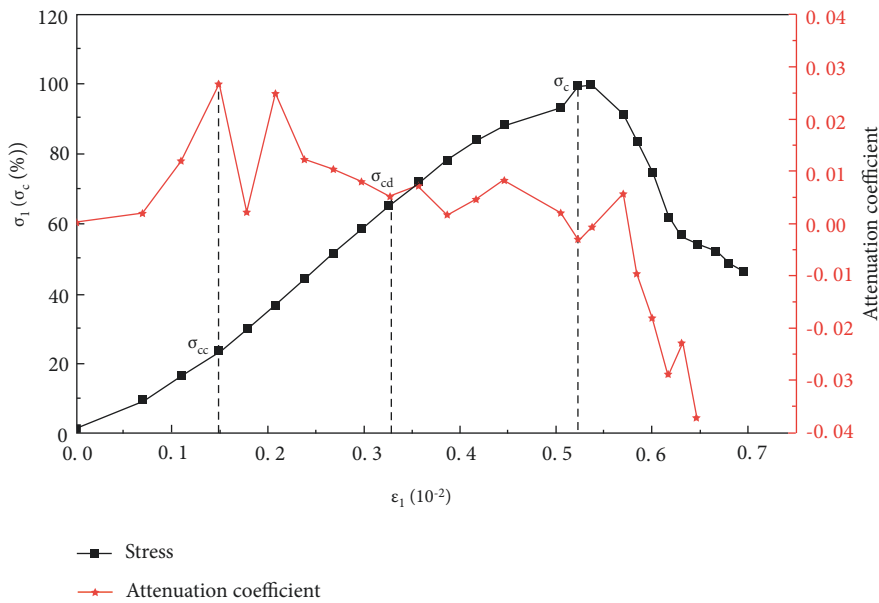
where  $A_0$  and  $A$  are the amplitudes of the first ultrasonic wave before and after loading, respectively, and  $d$  is propagation distance.

The back-filling concrete specimens were monogenetic and anisotropic, and the degree of the development of the internal joints and microcracks differed under different stress states, causing clearly evident diffraction or reflection of the ultrasonic wave, and therefore, causing significant energy attenuation and ultrasonic spectrum distortion. Figure 9 shows the relationship between the received ultrasonic amplitude, attenuation coefficient, and stress level. During the staged loading process, the ultrasonic amplitude and energy attenuation coefficient increased at first and then decreased, and both were positively correlated with the stress level. Moreover, the ultrasonic amplitude was negatively correlated with the energy attenuation coefficient. At the initial loading stage of sample 3, the compaction and closure of the original fissures reduced the reflection or scattering attenuation during the propagation of the ultrasonic signal. The received amplitude, firstly, increased and then remained at a stable level. At the same time, the distance between the transmitting end and the receiving end decreased, causing the energy attenuation coefficient to rise linearly from 0 to its highest value of 0.026. At this point, the stress value was 8.90 MPa, or 23.3% of peak stress  $\sigma_c$ , and 6.7% different from crack closure stress  $\sigma_{cc}$  determined by the stress-strain curve. As the load increased, the specimen entered the elastic deformation stage where the microcracks developed in a stable manner. The amplitude of the received wave gradually increased with increasing stress. The development of internal microcracks led to an increase in diffraction attenuation. The energy attenuation coefficient decreased slowly from the maximum value. Stress at the inflection point of the curve was 27.48 MPa, or 72.0% of peak stress  $\sigma_c$ . It is consistent with damage stress  $\sigma_{cd}$  determined by the stress-strain curve. As the load was further increased, the internal microfractures of the specimen continued to accumulate, and the number of secondary cracks gradually increased. The ultrasonic signal amplitude began to decrease. Energy attenuation intensified, and the attenuation coefficient dropped sharply to 0. The stress value reached 37.84 MPa, or 99.2% of peak stress  $\sigma_c$ . Eventually, a macroscopic penetration crack appeared, and the specimen's bearing capacity diminished.

(2) *CV of the Dominant Frequency.* Fast Fourier Transform (FFT) spectrum analysis is a waveform signal analysis algorithm widely used to study the global spectral



(a)



(b)

FIGURE 9: Relational curve between ultrasonic receiving amplitude. (a) Attenuation coefficient (b) of concrete sample and stress level.

characteristics of a signal [20–26]. FFT was used to extract the amplitude and frequency characteristic parameters of the received signal at different loading levels. Because of the development of microcracks in the concrete specimens, the energy was distributed at the dominant and secondary frequencies during ultrasonic propagation, and the ratio between the maximum amplitude of the secondary frequency and that of the dominant frequency is defined as the CV of the dominant frequency.

$$\gamma = \frac{A_p}{A_s}, \tag{4}$$

where  $\gamma$  is the coefficient of the variation of the dominant frequency,  $A_p$  is the maximum amplitude of the dominant frequency of the received wave spectrum during the loading process, and  $A_s$  is the maximum amplitude of the secondary frequency of the received wave spectrum during the loading process.



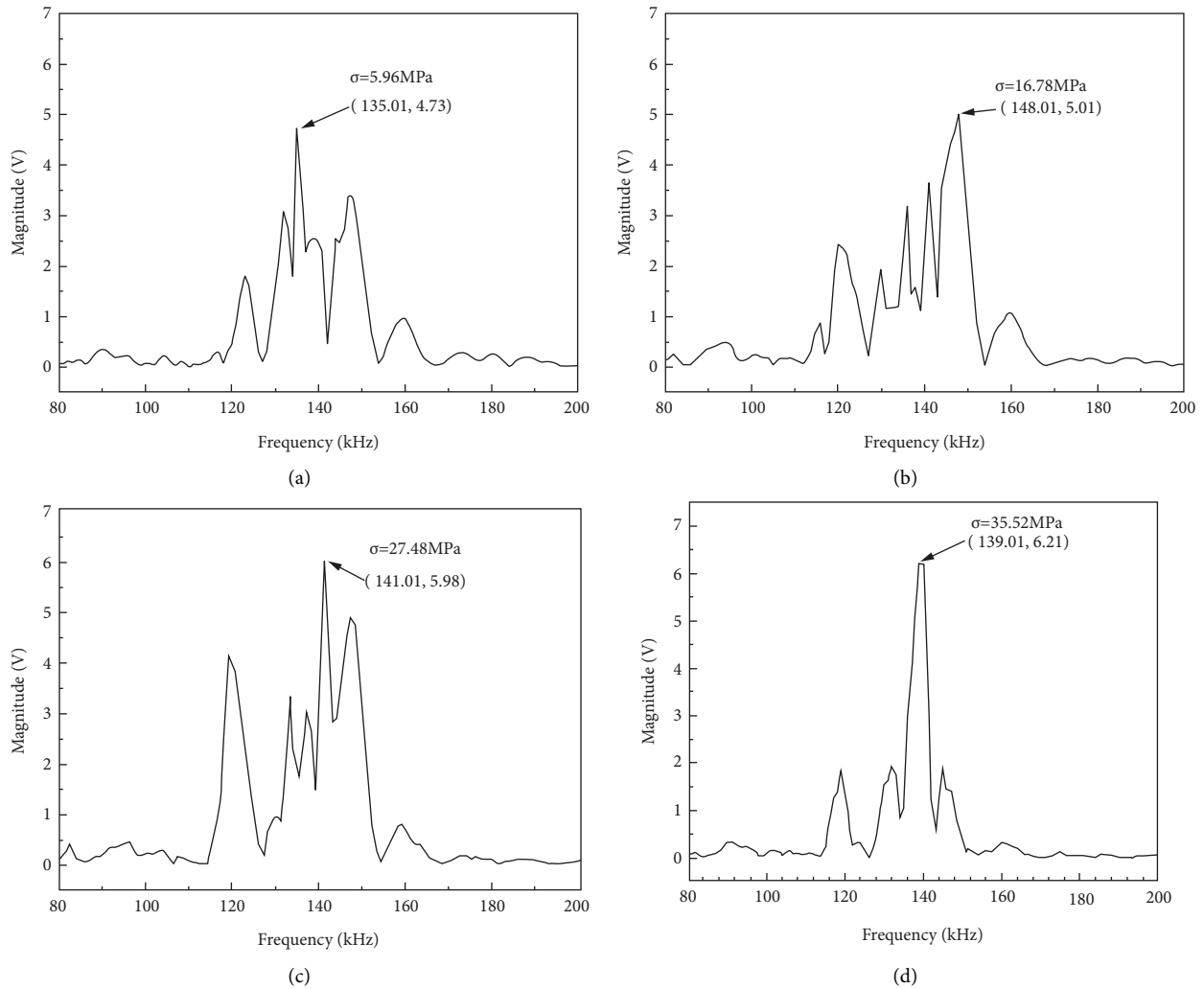


FIGURE 10: Two-dimensional spectrum of received ultrasonic signals at different stress levels. (a) 5.96 MPa. (b)  $\sigma = 16.78$  MPa. (c)  $\sigma = 27.48$  MPa. (d)  $\sigma = 35.52$  MPa.

Figure 10 shows the two-dimensional frequency spectrum characteristics of the received wave under different stress levels. The ultrasonic signal with the same dominant frequency was excited at these different stress levels. The received dominant frequency fluctuated around the transmitted frequency at 140 kHz, within a range of 110~170 kHz. As the load increased, the microfissures inside the specimens closed, developed, and expanded, and the dominant frequency variation of the received wave signal shows phased characteristics accordingly. The frequency distribution characteristics of the received signal were closely related to the development of internal fissures.

Figure 11 shows the CV curve of the dominant frequency of the received signal at different stress levels. In the initial loading stage, the irregular microfissure inside is pressed and closed, and the dominant frequency was largely distributed at 135~147 kHz with low amplitude. The variation coefficient of dominant frequency showed a small increase.

In the elastic deformation stage, because of the initiation and development of microcracks in the specimens, there were obvious multippeak distribution characteristics in the spectrum. The dominant frequency changed in the range of 120~170 kHz, and amplitude gradually increased. At this stage, both large- and small-scale cracks in the concrete specimens developed steadily, and the variation coefficient of dominant frequency fluctuates obviously. In the later part of the elastic deformation stage, the stress value was 24.84~27.84 MPa, the dominant frequency of the received signal varied between 140 and 150 kHz, and the amplitude reached its maximum value. The CV of the dominant frequency reached a maximum of 0.99, and the specimen entered the stable crack-expansion stage. When the stress value reached 35.52 MPa or 93.1% of peak stress  $\sigma_c$ , the high-frequency signal attenuated greatly, and there was only a single dominant frequency at about 140 kHz. The CV reached its minimum value of 0.29, through-cracks formed, and the overall specimen was damaged.

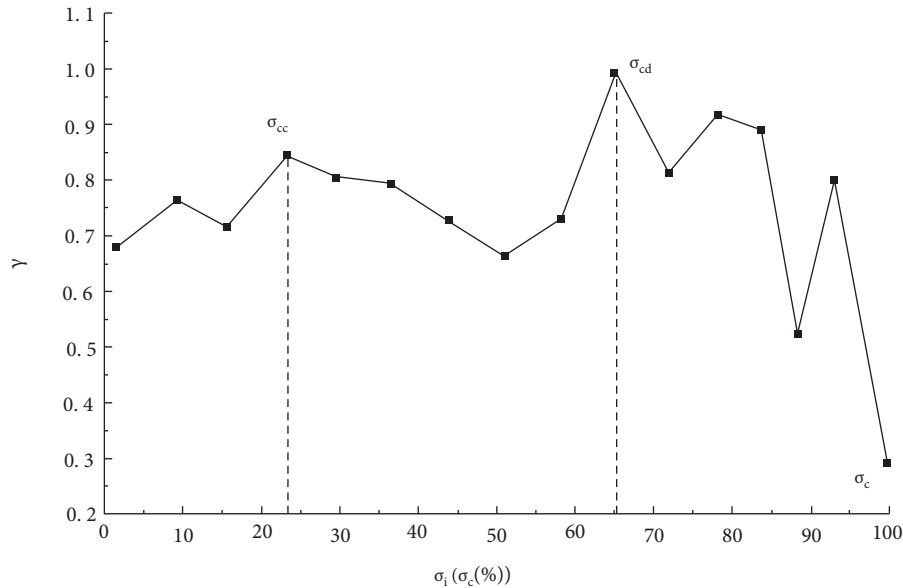


FIGURE 11: Variation coefficient curve of dominant frequency of received signals at different stress levels.

#### 4. Conclusions

In the paper, the propagation of an ultrasonic wave in back-filling concrete for gob-side entry retaining under staged loading conditions is studied. The time-frequency response characteristics of the magnitude and main frequency are obtained from the received ultrasonic wave in back-filling concrete with the different loading and damage stage. From the performed laboratory testing, the conclusions obtained are as follows:

- (1) The wave velocity, firstly, increased and then decreased with increasing loading. The damage factor determined by the ultrasonic wave velocity was able to reflect the crack expansion and the damage accumulation process of the concrete specimens. The macroscopic deformation characteristics and internal crack development all showed clear stage characteristics.
- (2) The magnitude and frequency spectrums of ultrasonic waves are sensitive to the damage evolution of the back-filling concrete specimen. The ultrasonic amplitude was positively correlated with the load-bearing capacity of the specimen. The amplitude in the late loading stage decreased significantly with the formation of macroscopic cracks.
- (3) The frequency of the received signal showed staged characteristics, and the CV of the dominant frequency first increased and then decreased. As loading increased, the dominant frequency of the received ultrasonic wave fluctuated around the transmission frequency of 140 kHz, within a range of 110~170 kHz. Late in the elastic deformation stage, fissures developed, and the dominant frequency bands of the ultrasonic wave were characterized by multippeak distribution. In the macroscopic crack

development stage, the high-frequency signal attenuated markedly, and the CV of the dominant frequency reached its minimum.

As a result, the magnitude and frequency spectrum of an ultrasonic *P*-wave can be capable of well-characterizing the damage accumulation and load-bearing capacity deterioration of concrete specimens. However, the new findings are limited under the triaxial loading cyclic loading conditions. In the future, the accuracy and universality under different loading paths using the ultrasonic *P*-wave should be further studied.[25, 26].

#### Data Availability

All data used to support the findings of this study are included within the article.

#### Conflicts of Interest

The authors declare that there are no conflicts of interest regarding publication of this paper.

#### Acknowledgments

Supported by the Key Program of National Natural Science Foundation of China (Program No. 51634007), Natural Science Basic Research Program of Shaanxi (Program No. 2021JLM-10), and Natural Science Basic Research Program of Shandong (Program No. 2019JZZY020326).

#### References

- [1] Y. Chen, B Jianbiao, T. Zhu, S. Yan, S.-H. Zhao, and X.-C. Li, "Mechanisms of roadside support in gob-side entry retaining and its application," *Rock and Soil Mechanics*, vol. 33, no. 5, pp. 1427-1432, 2012.

- [2] N. Zhang, H. Changliang, H. Jia-guang, and X.-G. Zheng, "Theory and practice of surrounding rock control for pillarless gob-side entry retaining," *Journal of China Coal Society*, vol. 39, no. 8, pp. 1635–1641, 2014.
- [3] W. Wang, G. Mingzhong, M. Wang et al., "Study on characteristics of deformation and stress distribution of gob-side entry retaining in the ultra-deep mine," *Chinese Journal of Rock Mechanics and Engineering*, vol. 38, no. S1, pp. 2955–2963, 2019.
- [4] H. Ming-ming, Z. Hui, Y.-H. Zhang et al., "Analysis of supporting resistance of reserved pier column for gob-side entry retaining in wide roadway," *Rock and Soil Mechanics*, vol. 39, no. 11, pp. 4218–4225, 2018.
- [5] F. Wang, J. Shang, B. Zhao, and Q. Cao, "Surrounding rock structural characteristics and its anchor-cable strengthened support technology for the gob-side entry retaining with roof cutting and pressure releasing," *Chinese Journal of Rock Mechanics and Engineering*, vol. 40, no. 11, pp. 2296–2305, 2021.
- [6] X. Deng, D. Chaowei, Z. Yuan, Z. Nan, and Y. Wei, "Deformation behavior of gob-side filling body of gob-side retaining entry in the deep back-filling workface," *Journal of Mining & Safety Engineering*, vol. 37, no. 1, pp. 62–72, 2020.
- [7] Y. Huang, J. Zhang, and F. Ju, "Technology of roadside packing in gob-side entry retaining and law of rock pressure," *Journal of Xi'an University of Science and Technology*, vol. 29, no. 5, pp. 515–520, 2009.
- [8] K. Jia-guang, N. Zhang, L. Bao-yu, and S. Guang-yao, "Analysis of supporting resistance of back-filling wall for gob-side entry retaining under typical roof conditions," *Rock and Soil Mechanics*, vol. 32, no. 9, pp. 2778–2784, 2011.
- [9] F. Guorui, Y. Ren, P. Wang et al., "Stress distribution and deformation characteristics of roadside backfill body for gob-side entry of fully-mechanized caving in thick coal seam," *Journal of Mining & Safety Engineering*, vol. 36, no. 6, pp. 1109–1119, 2019.
- [10] Y. Chen, M. Ning kang, Y. Yugui, and H. Shengpeng, "Research on stability control technology of filling body in Gob-side entry retaining," *Coal Science and Technology*, vol. 47, no. 9, pp. 273–278, 2019.
- [11] C. Han, N. Zhang, Z. Ran, R. Gao, and H. Yang, "Superposed disturbance mechanism of sequential overlying strata collapse for gob-side entry retaining and corresponding control strategies," *Journal of Central South University*, vol. 25, no. 9, pp. 2258–2271, 2018.
- [12] H. Shengpeng, *Study on Stability Mechanism of Back-Filling Body in Gob-Side Entry Retaining*, China University of Mining and Technology, Beijing, China, 2017.
- [13] X. L. Li, S. J. Chen, S. Wang, M. Zhao, and H. Liu, "Study on in situ stress distribution law of the deep mine taking Linyi Mining area as an example," *Advances in Materials Science and Engineering*, vol. 2021, no. 9, 11 pages, Article ID 5594181, 2021.
- [14] H. Y. Liu, B. Y. Zhang, X. L. Li et al., "Research on roof damage mechanism and control technology of gob-side entry retaining under close distance gob," *Engineering Failure Analysis*, vol. 138, no. 5, Article ID 106331, 2022.
- [15] M. Shengjun, Z. Liu, X. Zhao, and H. Zhengjun, "Energy dissipation and damage characteristics of Beishan granite under cyclic loading and unloading," *Chinese Journal of Rock Mechanics and Engineering*, vol. 40, no. 5, pp. 928–938, 2021.
- [16] X. Liu, H. Qijun, H. Ankui, and Z. Yu, "Study on determination of uniaxial characteristic stress of coal rock under quasi-static strain rate," *Chinese Journal of Rock Mechanics and Engineering*, vol. 39, no. 10, pp. 2038–2046, 2020.
- [17] C. D. Martin and N. A. Chandler, "The progressive fracture of Lac du Bonnet granite," *International Journal of Rock Mechanics and Mining Sciences & Geomechanics Abstracts*, vol. 31, no. 6, pp. 643–659, 1994.
- [18] P. Zhang, Z. Chengye, L. Tenghui, H. Jiqun, and Z. Rui, "Experimental study on the variation of wave velocity and energy evolution during tri-axial loading process of red sandstone," *Chinese Journal of Rock Mechanics and Engineering*, vol. 40, no. 7, pp. 1369–1382, 2021.
- [19] A. Cheng, D. Shunyi, Y. Zhang, H. Shibing, and Y. Zuyang, "Study on size effect of damage evolution of cemented backfill," *Chinese Journal of Rock Mechanics and Engineering*, vol. 38, no. S1, pp. 3053–3060, 2019.
- [20] T. Zhang, L. Zhang, L. I. Shugang, L. Jialei, J. Xiang, and P. Hongyu, "Characteristics of wave velocity and power spectral density of hole-containing specimens under water conditions," *Journal of China Coal Society*, vol. 43, no. 12, pp. 3387–3394, 2018.
- [21] C.-Y. Wang, X.-K. Chang, L. Yi-Lin, and G. Wenbin, "Spectrum evolution characteristics of acoustic emission during the rupture process of marble under uniaxial compression condition," *Rock and Soil Mechanics*, vol. 41, no. S1, pp. 51–62, 2020.
- [22] M. N. Toksöz, D. H. Johnston, and A. Timur, "Attenuation of seismic waves in dry and saturated rocks: I. Laboratory measurements," *Geophysics*, vol. 44, no. 4, pp. 681–690, 1979.
- [23] S. Ren, T. Han, and F. U. Liyun, "Theoretical and experimental study of P-wave attenuation in partially saturated sand stones under different pressures," *Chinese Journal of Geophysics*, vol. 63, no. 7, pp. 2722–2736, 2020.
- [24] B. Yan, W. Zhu, C. Hou, E. Yilmaz, and M. Saadat, "Characterization of early age behavior of cemented paste backfill through the magnitude and frequency spectrum of ultrasonic P-wave," *Construction and Building Materials*, vol. 249, Article ID 118733, 2020.
- [25] E. L. Hamilton, "Compressional wave attenuation in marine sediments," *Geophysics*, vol. 37, no. 4, pp. 620–646, 1972.
- [26] X. Li, S. Chen, S. Liu, and Z. Li, "AE waveform characteristics of rock mass under uniaxial loading based on Hilbert-Huang transform," *Journal of Central South University*, vol. 28, no. 6, pp. 1843–1856, 2021.